

# Sonosensitizers with Various Imaging Functions

Subjects: Medicine, General & Internal

Contributor: Mingxin Zhang, Yunlong Liang, Mingzhen Zhang, Yujie Zhang

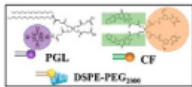
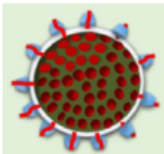
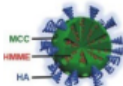
With the rapid development of sonodynamic therapy (SDT), sonosensitizers have evolved from traditional treatments to comprehensive diagnostics and therapies. Sonosensitizers play a crucial role in the integration of ultrasound imaging (USI), X-ray computed tomography (CT), and magnetic resonance imaging (MRI) diagnostics while also playing a therapeutic role.

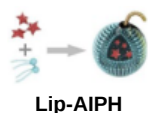
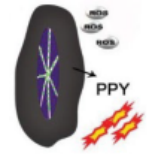
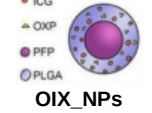
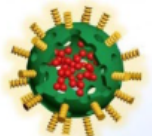
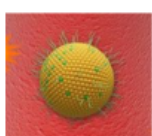

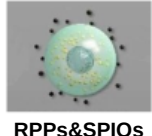
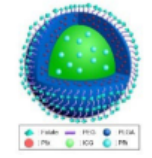
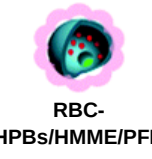
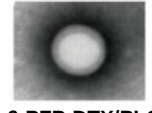
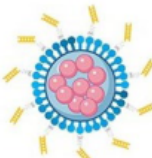
Keywords: sonodynamic therapy ; sonosensitizers ; clinical

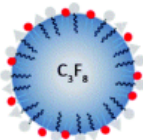
## 1. Contrast-Enhanced Ultrasound (CEUS)

Ultrasound (US) is a sound wave with a frequency of more than 20,000 Hz that is inaudible to the human ear. Ultrasound has the advantages of low-cost, simple, rapid, non-invasive, non-radioactive, accurate, continuous, dynamic, and repeatable scans [1][2][3]. Using the physical properties of ultrasound, various cross-sectional images of organs and surrounding organs can be displayed, which is close to the anatomical real structure. Therefore, ultrasound is often used as the first choice for the examination of solid organs and fluid-containing organs. In particular, ultrasound elastography and contrast-enhanced ultrasound (CEUS) are well established as being used for diagnosis. In CEUS, intravenously injected microbubbles are excited by longitudinal ultrasound in the examined area, producing nonlinear oscillations. The corresponding contrast agent software can distinguish the diseased tissues from the received contrast agent signals [4]. However, currently, 78.5% of radiology departments use diagnostic ultrasound imaging as a routine diagnostic imaging method, while only 26% of them use contrast-enhanced ultrasound [4]. The excessively expensive price of ultrasound contrast agents and their lower selectivity limited the clinical application of CEUS. It was found that some sonosensitizers used for SDT treatment also showed promising results in CEUS. **Table 1** lists the sonosensitizers and imaging capabilities used for CEUS imaging. Sonosensitizers produce stable microbubbles (MBs) or nanobubbles (NBs) under CEUS cavitation to achieve enhanced imaging [5][6][7]. Sonosensitizers achieve synergistic drug delivery and tumor therapy by affecting the lesion's tissue structure. Therefore, with the development of sonosensitizers, the clinical application of contrast-enhanced ultrasound is becoming more and more broad.

**Table 1.** US Imaging Characteristics of the Multifunctional Sonosensitizers.

| Sonosensitizers  | Probes  | Biological Model                      | SDT Result  | Imaging Effect  | Ref. |
|--|---------|---------------------------------------|---|---|------|
| <br>PCF-MBs     | PCF     | HT-29 cancer-bearing Balb/c nude mice | tumor inhibition rate of more than 50%                                | 20 s post-injection, the US imaging signal reached the maximum; and the contrast enhancement could last for more than 3 min | [8]  |
| <br>FMSN-DOX    | FMSNs   | TRAMP tumor-bearing nude mice         | The gradual reduction in tumor growth                                 | from day 1 to day 9 with significant contrast enhancement within the tumor.   | [9]  |
| <br>HMME/MCC-HA | MCC NPs | MCF-7 tumor-bearing nude mice         | successfully suppressed the tumor volume with the V/V0 of 0.87 ± 0.13 | strong US signals in tumor site at 3 h post-injection, and particularly after exposure to US stimulus                       | [10] |

| Sonosensitizers  | Probes            | Biological Model                                     | SDT Result  | Imaging Effect   | Ref. |
|--|-------------------|--|---|--|------|
| <br>Lip-AIPH                      | AIPH              | MCF-7 tumor-bearing mice                             | a highly significant antitumor effect was achieved in mice in the group of Lip-AIPH with US irradiation | a highly significant antitumor effect was achieved in mice in the group of Lip-AIPH with US irradiation              | [11] |
| <br>mTiO <sub>2</sub> @PPY-HNK    | mTiO <sub>2</sub> | 4T1 tumor model                                      | significantly inhibit the tumor growth  | as the concentration increases, the ultrasound signal is more intense and the image is clearer                       | [12] |
| <br>OIX_NPs                       | PFP               | ID8 cells into the left shoulder (the primary tumor) | significant inhibition of tumor volume  | peaking at 4 h post-injection.   | [13] |
| <br>TPZ/HMTNPs-SNO                | HMTNPs-SNO        | MCF-7 tumor-bearing nude mice                        | exhibited an effective therapeutic effect   | compared with the saline group, showed local enhancement at the tumor site.  | [14] |
| <br>IR780-NDs                     | PFP               | breast cancer 4T1 nude mice                          | Tumor weight drop   | 24 h after the injection of IR780-NDs a bright US signal occurred at the tumor site.                                 | [15] |
| <br>SMISO NPs                   | SMISO             | 4T1 tumor-bearing nude mice                          | the inhibition rate of tumor growth in the SMISO + US group reached 88.2%                               | the grayscale values of US images increase with them. concentration increases  | [16] |
| <br>RPPs&SPIOs                  | RPPs              | 4T1 tumors   | a 100% survival rate of mice at 90 days   | Shift in RPPs after thermal stimulation results in significant contrast enhancement                                  | [17] |
| <br>FA-PEG-PLGA-Ptx@ICG-Pfh NPs | Pfh               | MDA-MB231 tumor-bearing mice                         | tumor growth was significantly inhibited  | images were greatly improved   | [18] |
| <br>RBC-HPBs/HMME/PFH           | PFH               | 4T1 tumor-bearing female mice                        | enhancing tumor treatment effects of HMME   | A clear US signal was observed at 4 h after injection, and the strongest signal appeared at 8 h.                     | [19] |
| <br>Ce6-PFP-DTX/PLGA            | PFP               | breast cancer 4T1 nude mice                          | much higher inhibition rate of the CPDP NPs + LIFU group  | after LIFU irradiation, the corresponding intensity of CPDP NPs was elevated compared with the pre-irradiation group | [20] |
| <br>AS1411-DOX-PFH-PEG@PLGA     | PFH               | breast cancer 4T1 nude mice                          | the tumor volumes significantly decreased   | Increased imaging ability of ADPPs in vivo within 24 h after intravenous injection                                   | [21] |

| Sonosensitizers   | Probes | Biological Model        | SDT Result | Imaging Effect  | Ref. |
|---|--------|-------------------------|------------|---|------|
| <br>RB-MBs | MBs    | HT-29 tumor mouse model | -          | a contrast-enhanced ultrasound imaging mode at a frequency of 5 MHz | [22] |

Chen M. et al. [8] reported a liposomal nanoparticle based on porphyrin/camptothecin-floxuridine triad microbubbles (PCF-MBs). The novel PCF-MB not only realized ultrasound imaging but also achieved chemo-photodynamic combination therapy. After intravenously injecting 1 mg/mL of PCF-MBs into Balb/c nude mice bearing HT-29 colon cancer, the ability of PCF-MBs to potentiate ultrasound imaging was investigated by a fixed-frequency ultrasound transducer. The results showed that before the injection, there was hardly any sonographic signal in the tumor. The ultrasound imaging signals peaked 20 s after injection, and the peak state lasted more than 3 min.


Zhang et al. [16] synthesized a composite system in which Mn-doped  $\text{In}_2\text{S}_3/\text{InOOH}$  (SMISO) is loaded in spinodal silica ( $\text{r-SiO}_2$ ) to integrate ultrasound imaging and SDT for the detection and treatment of breast cancer. The live Type B US imaging results showed that the grayscale was changed after injection of  $\text{SiO}_2$ , MISO, or SMISO solutions in the 4T1 breast tumor model, and there was a statistical difference between SMISO and the control group ( $p < 0.01$ ), suggesting SMISO could achieve ultrasound imaging. Further, it was found that the signal intensity increased after SMISO NPs injection and peaked at 12 h, guiding the optimal time for ultrasound irradiation. And then, 12 h after the NPs injection, the signal intensity gradually decreased until it disappeared, indicating that the NPs were eliminated from the tumor. Under US irradiation, the SMISO NPs effectively inhibited tumor growth. In summary, the nanoplatform simultaneously had therapeutic efficacy and imaging capability.


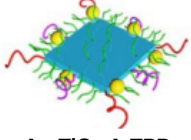
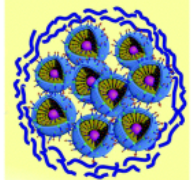
Zhang L et al. [15] fabricated an innovative nanoplatform capable of multimodal (FLI/PAI/USI) imaging using IR780 and perfluoropentane (PFP), as well as guiding SDT for tumor treatment. After intravenous injection of IR780-NDs, researchers acquired enhanced ultrasound images of xenograft tumors in nude mice with 4T1 breast cancer. At 24 h after administration in the caudal i.v., the US signal in CEUS mode showed brightness. In addition, the quantification data indicated that the echo intensity was much stronger in the post-injection group than in the pre-injection group.

## 2. X-ray Computed Tomography (CT)

CT scanning utilizes a computer to process a combination of several X-ray images acquired from different angulations to develop an anatomical picture of the scanned object [23]. CT has become a popular noninvasive clinical imaging method because of its reproducibility, low price, and ease of use [24]. CT scans are divided into conventional and enhanced scans according to whether contrast media is used or not. Since plain CT cannot distinguish between tissues with similar mass attenuation coefficients (e.g., normal organs and tumors), exogenous X-ray attenuating CT contrast materials need to be injected intravenously to identify diseased tissues. Iodine contrast is commonly used in clinical practice but has the following limitations: (1) susceptibility to allergic reactions and nephrotoxicity; (2) low dose-efficiency ratio; and (3) lack of targeting. Studies have investigated the utilization of sonosensitizers as CT imaging agents to overcome the shortcomings of commonly used clinical contrast agents. **Table 2** lists the sonosensitizers and imaging capabilities used for CT imaging.

**Table 2.** CT Imaging Characteristics of the Multifunctional Sonosensitizers.

| Sonosensitizers   | Probes             | Biological Model       | Treatment Result  | Imaging Effect   | Ref. |
|---|--------------------|------------------------|-------------------|--|------|
| <br>MnWO <sub>x</sub> -PEG | W(CO) <sub>6</sub> | 4T1 tumor-bearing mice | Tumor weight drop | CT imaging signal intensity was almost 2.4 times higher than that of the control group | [25] |

| Sonosensitizers   | Probes               | Biological Model            | Treatment Result   | Imaging Effect   | Ref. |
|---|----------------------|-----------------------------|--|--|------|
| <br>ABS-FA<br>AgBiS <sub>2</sub> @DSPE-PEG <sub>2000</sub> -FA | AgBiS <sub>2</sub>   | HeLa tumor-bearing mice     | Tumor size drop  | The CT signal intensity at the tumor site gradually increased and peaked at 6h after the injection | [26] |
| <br>Au-TiO <sub>2</sub> -A-TPP                                 | Au-TiO <sub>2</sub>  | MCF-7 tumor-bearing mice    | Tumor weight drop  | The CT signal in the tumor area reached its maximum at 24 h  | [27] |
| <br>GMCDs-FA@CMC   | Au@mSiO <sub>2</sub> | orthotopic colorectal tumor | Decreased number and smaller diameter of colorectal tumors | The nanoprobe remained in the colorectal region  | [28] |

Cao et al. [27] designed and synthesized titanium oxide (TiO<sub>2</sub>) nanosheets with triphenylphosphine (TPP) and AS1411 aptamer structure to realize mitochondria-targeted, CT imaging, and sonodynamic-chemotherapy for cancer treatment. Relative to the control group, Au-TiO<sub>2</sub>-A-TPP-treated mice displayed significant CT signals at the tumor sites, which validated the capability of Au-TiO<sub>2</sub>-A-TPP to diagnose tumors by CT imaging in vivo. As the concentration of Au-TiO<sub>2</sub>-A-TPP increased, the brightness and CT values of CT images increased, suggesting a linear relationship between CT grayscale values and concentration. As mentioned previously, contrast agents commonly used in clinical practice may not be appropriate for patients with renal insufficiency, who may be better suited for contrast agents with a short half-life in vivo and low nephrotoxicity. Surprisingly, the half-life of Au-TiO<sub>2</sub>-A-TPP in the blood circulation of mice was only 4.71 h, indicating Au-TiO<sub>2</sub>-A-TPP was very promising for patients with renal insufficiency.

Cheng K et al. [26] developed an AgBiS<sub>2</sub>@DSPE-PEG2000-FA (ABS-FA) with good biosafety and active targeted CT imaging capability that combined photothermal and ultrasound kinetic treatment capabilities. It was found that ABS-FA had significant targeting in tumor tissues in vivo, and the CT signals at the site of the tumor were steadily enhanced after ABS-FA (300  $\mu$ L, 5 mg/mL) injection, reaching a peak at 6–12 h. However, the non-targeted ABS-NH<sub>2</sub> signals did not change at different time points at the tumor site. The results of low-power (0.35 W/cm<sup>2</sup>) infrared thermography were consistent with those of CT, which showed that the thermal signal appeared 2 h after drug injection and reached its maximum 10 h after injection.

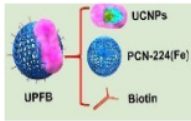



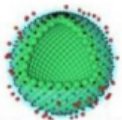
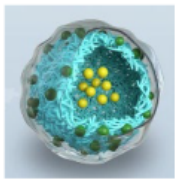
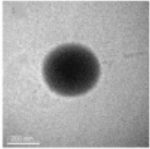
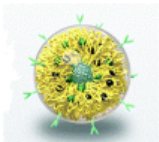
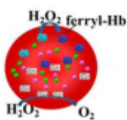
Zhang et al. [28] constructed a novel oral nanoparticle, Au@mSiO<sub>2</sub>/Ce6/DOX/SLB-FA@CMC (GMCDs-FA@CMC), that endowed the pH/ultrasonic dual-response to realize the combination of SDT with chemotherapy for colorectal cancer treatment. After oral delivery of GMCDs-FA@CMC, a well-defined tumor CT signal was observed in situ in colorectal cancer model mice and persisted for 7–9 h. It was found that the enteric-coated particles possessed good CT imaging effects in vivo by oral delivery and could be used to direct SDT-chemotherapy for colorectal cancer treatment.


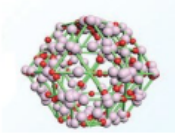
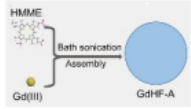
### 3. Magnetic Resonance Imaging (MRI)

Since the first implementation of MRI in 1973 as a non-invasive and multi-contrast detection method, MR imaging has been widely used in various biomedical fields [29]. MRI can reflect tissue lesions by combining parameters such as flow effects and electromagnetic wave-related proton density after the excitation of strong magnetic field pulses and the formation of magnetic resonance phenomena through hydrogen atoms in human water molecules [30]. The images are also processed with the aid of computer technology to obtain an excellent diagnosis of the pathology, which has high spatial and tissue resolution [31][32][33]. Therefore, it is extensively utilized clinically in the diagnosis and prognostic status of various diseases. Magnetic resonance imaging is not sensitive, but this obstacle can be overcome by exogenous contrast agents by decreasing the relaxation time of bulk water [33][34]. It was found that appropriate contrast agents are important for enhancing the susceptibility and specificity of diagnosis, enhancing the degree of signal contrast, and improving the resolution of soft tissue images for clinical application [29]. For example, with the help of gadolinium (Gd)-

based  $T_1$  agents, information about the boundaries of brain tumors can be observed more clearly [35]. In recent years, some new nuclear magnetic sensitizers containing Mn and Fe have been applied to MRI tumor imaging [36][37]. **Table 3** lists the sonosensitizers and imaging capabilities used for MRI imaging.

**Table 3.** MR Imaging Characteristics of the Multifunctional Sonosensitizers.

| Sonosensitizers  | Probes                   | Biological Model                        | SDT Result   | Imaging Effect  | Ref. |
|--|--------------------------|---|--|---|------|
|  <p>UPFB</p>                                    | MOFs (Fe <sup>3+</sup> ) | U14 tumor-bearing Kunming mice          | increased inhibition of tumor growth                 | enhanced T <sub>2</sub> contrast signal   | [37] |
|  <p>Fe-TiO<sub>2</sub> NDs</p>                  | Fe <sup>3+</sup>         | 4T1 tumor-bearing mice                  | better tumor inhibition                              | The brightening effect through the T <sub>1</sub> -weighted MR images                               | [38] |
|  <p>Fe-VS<sub>2</sub>-PEG</p>                   | Fe <sup>3+</sup>         | 4T1 cells subcutaneously in BALB/c mice | better treatment effect and a longer survival period | the tumor had an obvious brightening effect 24 h after i.v. injection (T <sub>1</sub> )             | [36] |
|  <p>OCN-PEG-(Ce6-Gd<sup>3+</sup>)/BNN6</p>      | Ga <sup>3+</sup>         | 4T1 tumor-bearing mice                  | the tumor suppression rate reached 63.2%             | The T <sub>1</sub> -weighted contrast effect was significantly enhanced                             | [39] |
|  <p>MnSiO<sub>3</sub>-Pt@BSA-Ce6(MPBC)</p>     | Mn <sup>2+</sup>         | U14 tumor-bearing Balb/c mice           | tumor growth inhibition                              | the T <sub>1</sub> -MR signal of the tumor enhanced   | [40] |
|  <p>MG@P NPs</p>                              | PMnC (Mn)                | 4T1 tumor-bearing mice                  | the tumor growth of Mice remarkably suppressed       | T <sub>1</sub> signal of the tumor region showed an increasing trend within 24 h and then decreased | [41] |
|  <p>F3-PLGA@MB/Gd NPs</p>                     | Gd-DTPA-BMA              | the nude mice bearing MDA-MB-231 tumors | induce tumor cell apoptosis                          | Linear signal dependence of T <sub>1</sub> intensity values   | [42] |
|  <p>Ang-IR780-MnO<sub>2</sub>-PLGA (AIMP)</p> | MnO <sub>2</sub>         | U87MG tumor-bearing mice                | enhanced SDT effect                                  | A linear relationship was shown between the 1/T <sub>1</sub> values and Mn concentration            | [43] |
|  <p>DOX/Mn-TPPS@RBCS</p>                      | Mn-TPPS                  | MCF-7 tumor-bearing nude mice           | Inhibit tumor growth                                 | T <sub>1</sub> -weighted MR imaging results in enhancement  | [44] |

| Sonosensitizers  | Probes           | Biological Model                       | SDT Result  | Imaging Effect  | Ref. |
|--|------------------|--|---|---|------|
| <br>MnTTP-HSA | MnTTP (Mn)       | MCF-7 tumor-bearing nude mice          | the best in completely inhibiting tumor   | a $T_1$ the positive signal at the tumor showed an increasing trend within 3 h and then gradually decreased | [45] |
| <br>mZMD      | MnO <sub>2</sub> | HeLa tumor xenograft-bearing nude mice | significant suppression effects   | the concentration of the NCs increased, the $T_1$ MR images became brighter and brighter                    | [46] |
| <br>GdHF-NDs  | Ga <sup>3+</sup> | CT26 tumor-bearing mice                | GdHF-NDs/PEG + US shows the most potent efficiency in tumor suppression (73.7%) | $T_1$ signal strength increased   | [31] |

Lei et al. [36] recommended iron-doped vanadium disulfide nanosheets (Fe-VS<sub>2</sub> NSs) as novel sonosensitizers modified with polyethylene glycol (PEG) to achieve the combination of SDT with chemodynamic therapy (CDT) for cancer therapy. Fe-VS<sub>2</sub>-PEG NSs have magnetic resonance imaging capability and strong tumor inhibitory in vivo. At 24 h after intravenous administration of Fe-VS<sub>2</sub>-PEG, MR imaging of the tumor demonstrated significant enhancement, and the quantitative analysis showed that signal strength was 2.04 times stronger than that before administration. In addition, the concentration of Fe-VS<sub>2</sub>-PEG NSs was positively correlated with MR signal intensity.

Wang et al. [37] designed and constructed Janus nanostructures called UPFB, consisting of upconversion nanoparticles (UCNPs) (NaYF<sub>4</sub>:20%Yb, 1%Tm@NaYF<sub>4</sub>:10% Yb@NaNdF<sub>4</sub>) and porphyrin-based metal organic frameworks (MOFs) (PCN-224(Fe)). UPFB promoted ROS production by GSH depletion and oxygen supply and realized the integration of SDT and chemodynamic therapy (CDT) for oncology treatment under MRI guidance. Compared with the UPF group, the UPFB group darkened overtime at the tumor site, indicating that the  $T_2$  contrast signal was enhanced and the accumulation of UPFB was in a time-related manner. UPFB was highly enriched in tumor tissues by quantitative analysis of the biodistribution of Zr and Fe elements by inductively coupled plasma mass spectrometry (ICP-MS)). Furthermore, the circulation half-life of UPFB was calculated to be 3.381 h. All these results suggested that the UPFB possessed excellent tumor target ability and could be utilized as a contrast agent for  $T_2$ -weighted.

Guan et al. [46] reported a novel biodegradable nanomaterial derived from a mesoporous zeolitic-imidazolate framework@MnO<sub>2</sub>/doxorubicin hydrochloride (ZIF-90@MnO<sub>2</sub>/DOX, mZMD NCs) to achieve  $T_1$ -weighted MRI-guided SDT/CDT/chemotherapy. It was found that the MR image brightness increased with the concentration of mZMD NCs. After 8 h of intravenous administration, the tumor region was significantly brighter for imaging, indicating that mZMD NCs can effectively aggregate at the tumor site and release Mn<sup>2+</sup> for  $T_1$ -weighted MR imaging. The mZMD NCs showed good biocompatibility and biosafety and effectively suppressed the growth of tumor cells.

## 4. Multi-Modal Imaging

All imaging methods have their disadvantages: MRI has the characteristics of long acquisition time and low space coverage; CT has the risk of ionizing radiation; and the US has limited penetration ability [47][48][49][50]. Single-modality imaging cannot meet the growing demand for accuracy and reliability in clinical diagnostics or clinical research [51]. The combined application of multiple testing techniques has become a hot research topic, complementing each other's advantages and realizing more precise diseases [52]. Compared with single-mode imaging, multimode imaging achieves multiple imaging functions through a single nanomaterial, providing a basis for accurate cancer diagnosis [53]. To date, several nanoparticle-based bimodal co-imaging materials have been reported to achieve better imaging and treatment.

Wang et al. [54] prepared hollow CoP@N-carbon@PEG (CPCs@PEG) nanospheres (~60 nm) as sonosensitizers to inhibit tumor growth by promoting ROS production under US irradiation. With the incorporation of cobalt ions, which had magnetic properties and X-ray attenuation coefficients, CPCs@PEG were capable of both CT and MRI. Further, the authors also performed MRI imaging studies in vivo using 4T1 tumor-bearing mice as a model. After the injection of CPC10@PEG, the contrast of the cancer site became darker. In addition, the researchers conducted a CT imaging capability study. With the increase in CPC10@PEG concentration, the CT signal was gradually enhanced. The



researchers also investigated the in vivo CT imaging capabilities of CPC10@PEG, which showed a significant increase in the brightness of the cancer site after intravenous injection compared with pre-injection.

Gong et al. [25] designed and prepared a novel high-performance multifunctional sonosensitizer built on ultramicroscopic oxygen-deficient bimetallic oxide  $\text{MnWO}_x$  nanoparticles for multimodal imaging-guided SDT for cancer therapy. The  $\text{MnWO}_x$ -PEG nanoparticles exhibited effective SDT effects by producing  $^1\text{O}_2$  and  $\cdot\text{OH}$  and possessed the glutathione depletion capability to enhance the SDT efficacy.  $\text{MnWO}_x$ -PEG exhibited good biosafety and excellent tumor growth suppression in mice under ultrasound irradiation. Due to the high attenuation of X-rays by the W element,  $\text{MnWO}_x$ -PEG can also be applied in CT imaging and as a reduction agent for  $\text{T}_1$  in magnetic resonance imaging. The findings indicated that after 24 h of intravenous injection of  $\text{MnWO}_x$ -PEG 4T1, the tumor-bearing mice showed significant CT (2.4 times) and MRI (1.8 times) signals in the tumor site. These multimodal imaging results demonstrated that  $\text{MnWO}_x$ -PEG can efficiently accumulate in tumors, and sonosensitizers had diagnostic imaging capabilities and assisted in the precise treatment of tumors with SDT.

---

## References

1. Ke, H.; Wang, J.; Dai, Z.; Jin, Y.; Qu, E.; Xing, Z.; Guo, C.; Yue, X.; Liu, J. Gold-nanoshelled microcapsules: A theranostic agent for ultrasound contrast imaging and photothermal therapy. *Angew. Chem.* 2011, 50, 3017–3021.
2. Slagle, C.J.; Thamm, D.H.; Randall, E.K.; Borden, M.A. Click Conjugation of Cloaked Peptide Ligands to Microbubbles. *Bioconjugate Chem.* 2018, 29, 1534–1543.
3. Wang, Y.; Cong, H.; Wang, S.; Yu, B.; Shen, Y. Development and application of ultrasound contrast agents in biomedicine. *J. Mater. Chem. B* 2021, 9, 7633–7661.
4. Kloth, C.; Kratzer, W.; Schmidberger, J.; Beer, M.; Clevert, D.A.; Graeter, T. Ultrasound 2020—Diagnostics & Therapy: On the Way to Multimodal Ultrasound: Contrast-Enhanced Ultrasound (CEUS), Microvascular Doppler Techniques, Fusion Imaging, Sonoelastography, Interventional Sonography. In *RöFo-Fortschritte auf dem Gebiet der Röntgenstrahlen und der Bildgebenden Verfahren*; Georg Thieme Verlag KG: Leipzig, Germany, 2021; Volume 193, pp. 23–32.
5. Claudon, M.; Dietrich, C.F.; Choi, B.I.; Cosgrove, D.O.; Kudo, M.; Nolsøe, C.P.; Piscaglia, F.; Wilson, S.R.; Barr, R.G.; Chammas, M.C.; et al. Guidelines and good clinical practice recommendations for Contrast Enhanced Ultrasound (CEUS) in the liver—Update 2012: A WFUMB-EFSUMB initiative in cooperation with representatives of AFSUMB, AIUM, ASUM, FLAUS and ICUS. *Ultrasound Med. Biol.* 2013, 39, 187–210.
6. Huynh, E.; Rajora, M.A.; Zheng, G. Multimodal micro, nano, and size conversion ultrasound agents for imaging and therapy. *Wiley Interdiscip. Rev. Nanomed. Nanobiotechnol.* 2016, 8, 796–813.
7. Sun, S.; Xu, Y.; Fu, P.; Chen, M.; Sun, S.; Zhao, R.; Wang, J.; Liang, X.; Wang, S. Ultrasound-targeted photodynamic and gene dual therapy for effectively inhibiting triple negative breast cancer by cationic porphyrin lipid microbubbles loaded with HIF1 $\alpha$ -siRNA. *Nanoscale* 2018, 10, 19945–19956.
8. Chen, M.; Liang, X.; Gao, C.; Zhao, R.; Zhang, N.; Wang, S.; Chen, W.; Zhao, B.; Wang, J.; Dai, Z. Ultrasound Triggered Conversion of Porphyrin/Camptothecin-Fluoroxymidine Triad Microbubbles into Nanoparticles Overcomes Multidrug Resistance in Colorectal Cancer. *ACS Nano* 2018, 12, 7312–7326.
9. Ho, Y.J.; Wu, C.H.; Jin, Q.F.; Lin, C.Y.; Chiang, P.H.; Wu, N.; Fan, C.H.; Yang, C.M.; Yeh, C.K. Superhydrophobic drug-loaded mesoporous silica nanoparticles capped with  $\beta$ -cyclodextrin for ultrasound image-guided combined antivasculature and chemo-sonodynamic therapy. *Biomaterials* 2020, 232, 119723.
10. Feng, Q.; Zhang, W.; Yang, X.; Li, Y.; Hao, Y.; Zhang, H.; Hou, L.; Zhang, Z. pH/Ultrasound Dual-Responsive Gas Generator for Ultrasound Imaging-Guided Therapeutic Inertial Cavitation and Sonodynamic Therapy. *Adv. Healthc. Mater.* 2018, 7, 1700957.
11. Lin, X.; Qiu, Y.; Song, L.; Chen, S.; Chen, X.; Huang, G.; Song, J.; Chen, X.; Yang, H. Ultrasound activation of liposomes for enhanced ultrasound imaging and synergistic gas and sonodynamic cancer therapy. *Nanoscale Horiz.* 2019, 4, 747–756.
12. He, Y.; Wan, J.; Yang, Y.; Yuan, P.; Yang, C.; Wang, Z.; Zhang, L. Multifunctional Polypyrrole-Coated Mesoporous  $\text{TiO}_2$  Nanocomposites for Photothermal, Sonodynamic, and Chemotherapeutic Treatments and Dual-Modal Ultrasound/Photoacoustic Imaging of Tumors. *Adv. Healthc. Mater.* 2019, 8, e1801254.
13. Zheng, J.; Sun, J.; Chen, J.; Zhu, S.; Chen, S.; Liu, Y.; Hao, L.; Wang, Z.; Chang, S. Oxygen and oxaliplatin-loaded nanoparticles combined with photo-sonodynamic inducing enhanced immunogenic cell death in syngeneic mouse models of ovarian cancer. *J. Control. Release* 2021, 332, 448–459.

14. Feng, Q.; Li, Y.; Yang, X.; Zhang, W.; Hao, Y.; Zhang, H.; Hou, L.; Zhang, Z. Hypoxia-specific therapeutic agents delivery nanotheranostics: A sequential strategy for ultrasound mediated on-demand tritherapies and imaging of cancer. *J. Control. Release* 2018, 275, 192–200.
15. Zhang, L.; Yi, H.; Song, J.; Huang, J.; Yang, K.; Tan, B.; Wang, D.; Yang, N.; Wang, Z.; Li, X. Mitochondria-Targeted and Ultrasound-Activated Nanodroplets for Enhanced Deep-Penetration Sonodynamic Cancer Therapy. *ACS Appl. Mater. Interfaces* 2019, 11, 9355–9366.
16. Zhang, T.; Zheng, Q.; Xie, C.; Fan, G.; Wang, Y.; Wu, Y.; Fu, Y.; Huang, J.; Craig, D.Q.M.; Cai, X.; et al. Integration of Silica Nanorattles with Manganese-Doped In<sub>2</sub>S<sub>3</sub>/InOOH to Enable Ultrasound-Mediated Tumor Theranostics. *ACS Appl. Mater. Interfaces* 2023, 15, 4883–4894.
17. Qin, Q.; Zhou, Y.; Li, P.; Liu, Y.; Deng, R.; Tang, R.; Wu, N.; Wan, L.; Ye, M.; Zhou, H.; et al. Phase-transition nanodroplets with immunomodulatory capabilities for potentiating mild magnetic hyperthermia to inhibit tumour proliferation and metastasis. *J. Nanobiotechnol.* 2023, 21, 131.
18. Liu, F.; Chen, Y.; Li, Y.; Guo, Y.; Cao, Y.; Li, P.; Wang, Z.; Gong, Y.; Ran, H. Folate-receptor-targeted laser-activable poly(lactide-co-glycolic acid) nanoparticles loaded with paclitaxel/indocyanine green for photoacoustic/ultrasound imaging and chemo/photothermal therapy. *Int. J. Nanomed.* 2018, 13, 5139–5158.
19. Zhang, H.; Chen, J.; Zhu, X.; Ren, Y.; Cao, F.; Zhu, L.; Hou, L.; Zhang, H.; Zhang, Z. Ultrasound induced phase-transition and invisible nanobomb for imaging-guided tumor sonodynamic therapy. *J. Mater. Chem. B* 2018, 6, 6108–6121.
20. Zhang, Q.; Wang, W.; Shen, H.; Tao, H.; Wu, Y.; Ma, L.; Yang, G.; Chang, R.; Wang, J.; Zhang, H.; et al. Low-Intensity Focused Ultrasound-Augmented Multifunctional Nanoparticles for Integrating Ultrasound Imaging and Synergistic Therapy of Metastatic Breast Cancer. *Nanoscale Res. Lett.* 2021, 16, 73.
21. Kang, Z.; Yang, M.; Feng, X.; Liao, H.; Zhang, Z.; Du, Y. Multifunctional Theranostic Nanoparticles for Enhanced Tumor Targeted Imaging and Synergistic FUS/Chemotherapy on Murine 4T1 Breast Cancer Cell. *Int. J. Nanomed.* 2022, 17, 2165–2187.
22. Hou, R.; Liang, X.; Li, X.; Zhang, X.; Ma, X.; Wang, F. In situ conversion of rose bengal microbubbles into nanoparticles for ultrasound imaging guided sonodynamic therapy with enhanced antitumor efficacy. *Biomater. Sci.* 2020, 8, 2526–2536.
23. Jiang, Z.; Zhang, M.; Li, P.; Wang, Y.; Fu, Q. Nanomaterial-based CT contrast agents and their applications in image-guided therapy. *Theranostics* 2023, 13, 483–509.
24. Pan, X.; Siewerdsen, J.; La Riviere, P.J.; Kalender, W.A. Anniversary paper. Development of x-ray computed tomography: The role of medical physics and AAPM from the 1970s to present. *Med. Phys.* 2008, 35, 3728–3739.
25. Gong, F.; Cheng, L.; Yang, N.; Betzer, O.; Feng, L.; Zhou, Q.; Li, Y.; Chen, R.; Popovtzer, R.; Liu, Z. Ultrasmall Oxygen-Deficient Bimetallic Oxide MnWOX Nanoparticles for Depletion of Endogenous GSH and Enhanced Sonodynamic Cancer Therapy. *Adv. Mater.* 2019, 31, e1900730.
26. Cheng, K.; Zhang, R.Y.; Yang, X.Q.; Zhang, X.S.; Zhang, F.; An, J.; Wang, Z.Y.; Dong, Y.; Liu, B.; Zhao, Y.D.; et al. One-for-All Nanoplatfrom for Synergistic Mild Cascade-Potentiated Ultrasound Therapy Induced with Targeting Imaging-Guided Photothermal Therapy. *ACS Appl. Mater. Interfaces* 2020, 12, 40052–40066.
27. Cao, Y.; Wu, T.; Dai, W.; Dong, H.; Zhang, X. TiO<sub>2</sub> Nanosheets with the Au Nanocrystal-Decorated Edge for Mitochondria-Targeting Enhanced Sonodynamic Therapy. *Chem. Mater.* 2019, 31, 9105–9114.
28. Zhang, R.Y.; Cheng, K.; Xuan, Y.; Yang, X.Q.; An, J.; Hu, Y.G.; Liu, B.; Zhao, Y.D. A pH/ultrasonic dual-response step-targeting enterosoluble granule for combined sonodynamic-chemotherapy guided via gastrointestinal tract imaging in orthotopic colorectal cancer. *Nanoscale* 2021, 13, 4278–4294.
29. Guo, L.; Xi, J.; Teng, J.; Wang, J.; Chen, Y. Magnetic Resonance Neuroimaging Contrast Agents of Nanomaterials. *Biomed. Res. Int.* 2022, 2022, 6790665.
30. Yuan, P.; Song, D. MRI tracing non-invasive TiO<sub>2</sub>-based nanoparticles activated by ultrasound for multi-mechanism therapy of prostatic cancer. *Nanotechnology* 2018, 29, 125101.
31. Geng, P.; Yu, N.; Liu, X.; Zhu, Q.; Wen, M.; Ren, Q.; Qiu, P.; Zhang, H.; Li, M.; Chen, Z. Sub 5 nm Gd<sup>3+</sup>-Hemoporphin Framework Nanodots for Augmented Sonodynamic Theranostics and Fast Renal Clearance. *Adv. Healthc. Mater.* 2021, 10, e2100703.
32. Geethanath, S.; Vaughan, J.T., Jr. Accessible magnetic resonance imaging: A review. *J. Magn. Reson. Imaging* 2019, 49, e65–e77.
33. Pellico, J.; Ellis, C.M.; Davis, J.J. Nanoparticle-Based Paramagnetic Contrast Agents for Magnetic Resonance Imaging. *Contrast Media Mol. Imaging* 2019, 2019, 1845637.



34. De León-Rodríguez, L.M.; Martins, A.F.; Pinho, M.C.; Rofsky, N.M.; Sherry, A.D. Basic MR relaxation mechanisms and contrast agent design. *J. Magn. Reson. Imaging* 2015, 42, 545–565.
35. Abd-Allah, M.K.; Awad, A.I.; Khalaf, A.A.M.; Hamed, H.F.A. A review on brain tumor diagnosis from MRI images: Practical implications, key achievements, and lessons learned. *Magn. Reson. Imaging* 2019, 61, 300–318.
36. Lei, H.; Wang, X.; Bai, S.; Gong, F.; Yang, N.; Gong, Y.; Hou, L.; Cao, M.; Liu, Z.; Cheng, L. Biodegradable Fe-Doped Vanadium Disulfide Theranostic Nanosheets for Enhanced Sonodynamic/Chemodynamic Therapy. *ACS Appl. Mater. Interfaces* 2020, 12, 52370–52382.
37. Wang, Z.; Liu, B.; Sun, Q.; Feng, L.; He, F.; Yang, P.; Gai, S.; Quan, Z.; Lin, J. Upconverted Metal-Organic Framework Janus Architecture for Near-Infrared and Ultrasound Co-Enhanced High Performance Tumor Therapy. *ACS Nano* 2021, 15, 12342–12357.
38. Bai, S.; Yang, N.; Wang, X.; Gong, F.; Dong, Z.; Gong, Y.; Liu, Z.; Cheng, L. Ultrasmall Iron-Doped Titanium Oxide Nanodots for Enhanced Sonodynamic and Chemodynamic Cancer Therapy. *ACS Nano* 2020, 14, 15119–15130.
39. Zheng, Y.; Liu, Y.; Wei, F.; Xiao, H.; Mou, J.; Wu, H.; Yang, S. Functionalized g-C<sub>3</sub>N<sub>4</sub> nanosheets for potential use in magnetic resonance imaging-guided sonodynamic and nitric oxide combination therapy. *Acta Biomater.* 2021, 121, 592–604.
40. Jiang, F.; Yang, C.; Ding, B.; Liang, S.; Zhao, Y.; Cheng, Z.; Liu, M.; Xing, B.; Ma, P.; Lin, J. Tumor microenvironment-responsive MnSiO<sub>3</sub>-Pt@BSA-Ce6 nanoplatform for synergistic catalysis-enhanced sonodynamic and chemodynamic cancer therapy. *Chin. Chem. Lett.* 2022, 33, 2959–2964.
41. Wang, J.; Huang, J.; Zhou, W.; Zhao, J.; Peng, Q.; Zhang, L.; Wang, Z.; Li, P.; Li, R. Hypoxia modulation by dual-drug nanoparticles for enhanced synergistic sonodynamic and starvation therapy. *J. Nanobiotechnol.* 2021, 19, 87.
42. Li, Y.; Hao, L.; Liu, F.; Yin, L.; Yan, S.; Zhao, H.; Ding, X.; Guo, Y.; Cao, Y.; Li, P.; et al. Cell penetrating peptide-modified nanoparticles for tumor targeted imaging and synergistic effect of sonodynamic/HIFU therapy. *Int. J. Nanomed.* 2019, 14, 5875–5894.
43. Liu, S.; Zhang, W.; Chen, Q.; Hou, J.; Wang, J.; Zhong, Y.; Wang, X.; Jiang, W.; Ran, H.; Guo, D. Multifunctional nanozyme for multimodal imaging-guided enhanced sonodynamic therapy by regulating the tumor microenvironment. *Nanoscale* 2021, 13, 14049–14066.
44. Du, B.; Yan, X.; Ding, X.; Wang, Q.; Du, Q.; Xu, T.; Shen, G.; Yao, H.; Zhou, J. Oxygen Self-Production Red Blood Cell Carrier System for MRI Mediated Cancer Therapy: Ferryl-Hb, Sonodynamic, and Chemical Therapy. *ACS Biomater. Sci. Eng.* 2018, 4, 4132–4143.
45. Wang, L.; Song, W.; Choi, S.; Yu, K.; Zhang, F.; Guo, W.; Ma, Y.; Wang, K.; Qu, F.; Lin, H. Hollow CoP@N-Carbon Nanospheres: Heterostructure and Glucose-Enhanced Charge Separation for Sonodynamic/Starvation Therapy. *ACS Appl. Mater. Interfaces* 2023, 15, 2552–2563.
46. Ma, A.; Chen, H.; Cui, Y.; Luo, Z.; Liang, R.; Wu, Z.; Chen, Z.; Yin, T.; Ni, J.; Zheng, M.; et al. Metalloporphyrin Complex-Based Nanosensitizers for Deep-Tissue Tumor Theranostics by Noninvasive Sonodynamic Therapy. *Small* 2019, 15, e1804028.
47. Guan, S.; Liu, X.; Li, C.; Wang, X.; Cao, D.; Wang, J.; Lin, L.; Lu, J.; Deng, G.; Hu, J. Intracellular Mutual Amplification of Oxidative Stress and Inhibition Multidrug Resistance for Enhanced Sonodynamic/Chemodynamic/Chemo Therapy. *Small* 2022, 18, e2107160.
48. Neuschmelting, V.; Harmsen, S.; Beziere, N.; Lockau, H.; Hsu, H.T.; Huang, R.; Razansky, D.; Ntziachristos, V.; Kircher, M.F. Dual-Modality Surface-Enhanced Resonance Raman Scattering and Multispectral Optoacoustic Tomography Nanoparticle Approach for Brain Tumor Delineation. *Small* 2018, 14, e1800740.
49. Salvatori, M.; Rizzo, A.; Rovera, G.; Indovina, L.; Schillaci, O. Radiation dose in nuclear medicine: The hybrid imaging. *Radiol. Med.* 2019, 124, 768–776.
50. Perry, J.L.; Mason, K.; Sutton, B.P.; Kuehn, D.P. Can Dynamic MRI Be Used to Accurately Identify Velopharyngeal Closure Patterns? *Cleft Palate-Craniofacial J.* 2018, 55, 499–507.
51. Guo, W.; Chen, Z.; Tan, L.; Gu, D.; Ren, X.; Fu, C.; Wu, Q.; Meng, X. Emerging biocompatible nanoplatforms for the potential application in diagnosis and therapy of deep tumors. *View* 2021, 3, 20200174.
52. Jennings, L.E.; Long, N.J. 'Two is better than one'--probes for dual-modality molecular imaging. *Chem. Commun.* 2009, 24, 3511–3524.
53. Lee, S.Y.; Jeon, S.I.; Jung, S.; Chung, I.J.; Ahn, C.H. Targeted multimodal imaging modalities. *Adv. Drug Deliv. Rev.* 2014, 76, 60–78.

54. Cai, W.; Chen, X. Multimodality molecular imaging of tumor angiogenesis. *J. Nucl. Med.* 2008, 49 (Suppl. 2), 113s–128s.
- 

Retrieved from <https://encyclopedia.pub/entry/history/show/118162>